Tunneling-assisted thermalization and recombination of nonequilibrium carriers in localized states: Application to the frequency-resolved drift mobility in amorphous silicon

K. Hattori, T. Hirao, Y. Musa, and H. Okamoto
Department of Physical Science, Graduate School of Engineering Science, Osaka University, Toyonaka, Osaka 560-8531, Japan
(Received 8 December 2000; revised manuscript received 12 February 2001; published 10 September 2001)

This article presents a theory for nonequilibrium carrier kinetics in amorphous semiconductors containing localized states among which finite interactions are allowed via tunneling. Fourier domain solutions are explored intensively in order to quantitatively interpret the frequency-dependent photocarrier drift mobility determined by modulated photoconductivity measurement. The theoretical analysis is in agreement with experiments carried out for hydrogenated amorphous silicon over a wide range of frequencies and temperatures, and discloses that the inclusion of tunneling transitions considerably accelerates carrier thermalization in localized band-tail states. A generalized recombination model that considers both direct capture of band carriers and tunneling transfer of band-tail carriers into recombination centers is also discussed in detail, suggesting that even for room temperature, the tunneling recombination takes place preferentially.

DOI: 10.1103/PhysRevB.64.125208 PACS number(s): 72.20.Jv, 71.23.An, 72.20.Fr, 71.23.Cq

I. INTRODUCTION

A fundamental property of amorphous semiconductors, such as hydrogenated amorphous silicon (a-Si:H), is the presence of localized gap states that significantly influence the relaxation of nonequilibrium carriers in these materials. Intensive effort has been devoted to understanding this process. However, existing models of carrier kinetics are too restrictive to account for all the experimental results although adequate agreement with some aspects was achieved in a limited range of temperature. For example, the multiple trapping model[1] is frequently used for the description of phenomena near room temperature. This model assumes, on the basis of Shockley-Read statistics, that carriers are trapped in localized states where they are immobile until thermally reemitted to extended states. Alternatively, the model that only takes into account carrier transitions between localized states via tunneling explains the experiments at lower temperatures.[2–8]

Recently, the authors introduced the modulated photoconductivity (MPC) technique for frequency-resolved measurement of the drift mobility of an ensemble of photocarriers.[9,10] The frequency-dependent drift mobility is related to its time-domain equivalent by Fourier transformation and intimately correlates with the energy distribution of nonequilibrium carriers in localized states. The frequency-domain assessment achieved by this experiment, which is free from the complexity often encountered in the time domain, where transient carrier distribution at any moment depends on the history of the decay, gives more straightforward access to the problem. The experimental results obtained for a-Si:H over a wide temperature range suggest that thermal transitions between localized and extended states as well as tunneling transitions between localized states contribute cooperatively to carrier dynamics. Motivated by this observation, as well as by the lack of theory with an extended scope, in the present study we pursue a theoretical analysis that treats all the probable transitions in a single unified model. Model predictions are in excellent agreement with drift-mobility experiments in a-Si:H. This leads to a quantitative evaluation of the carrier thermalization process in this material. An interesting conclusion regarding recombination via tunneling is also drawn from theoretical considerations.

The paper is organized as follows. The generalized theory for carrier thermalization and recombination is given in Sec. II. The numerical simulation and comparison with experiment are described in Sec. III. Finally we give a brief summary in Sec. IV.

II. THEORY OF CARRIER KINETICS

A. Thermalization

We begin by considering thermalization of nonequilibrium carriers of a single type in localized states distributed in space and in energy. In the following, we shall arbitrarily specify the carriers to be electrons. The treatment for holes is similar.

1. Rate equation

We base our theoretical analysis on the linearized rate equation

$$\frac{d}{dt}f_n(t)=n_c(t)C-f_n(t)e_n+\sum_m f_m(t)w_{mn}-f_n(t)\sum_m w_{nm}, \tag{1}$$

where $f_n(t)$ is the probability that state n is occupied by an electron at time t. The first two terms on the right-hand side of Eq. (1) describe the gain and loss of an electron due to capture from and thermal emission to the conduction band, respectively. The capture rate is expressed by the concentration of band electrons $n_c(t)$ multiplied by the coefficient C. A well-known detailed balance relation, $e_n=e(\varepsilon_n)=N_cC\exp[-(\varepsilon_c-\varepsilon_n)/kT]$, exists between the capture coefficient C and the thermal emission rate e_n for state n of energy ε_n, where N_c is the effective density of conduction-band states above energy ε_c and kT is the thermal energy.[11] The last two terms in Eq. (1) represent electron traffic among

localized states via tunneling transitions. The tunneling rate of an electron from an initial state n to a final state m, separated by a distance $|\mathbf{r}_m-\mathbf{r}_n|$ and by an energy $\varepsilon_m-\varepsilon_n$, is given to a good approximation by $w_{nm}=\nu(\varepsilon_m-\varepsilon_n)\exp(-2|\mathbf{r}_m-\mathbf{r}_n|/a)$, where a denotes the localization radius, and $\nu(\varepsilon)=\nu_0\exp[-\theta(\varepsilon)\varepsilon/kT]$; ν_0 is the frequency factor and $\theta(\varepsilon)$ the unit step function.[5–7] The tunneling rates obey a detailed balance between forward and backward processes and are symmetrized by a Boltzmann factor such that $w_{mn}/w_{nm}=\exp[-(\varepsilon_n-\varepsilon_m)/kT]$. The rate equation (1) does not contain the second-order terms appearing in its most general expression and assumes that the average occupancy of states is small. This would be a proper assumption for the conduction-band tail in intrinsic a-Si:H, details of which will be discussed in Sec. III.

The integral form of the linearized equation is easily shown to be

$$f_n(t)=\int_{-\infty}^{t}dt'\,n_cCs_n(t-t')+\sum_m\int_{-\infty}^{t}dt'\,f_m(t')w_{mn}s_n(t-t'). \tag{2}$$

This expression includes causality, that is, the occupation of each localized state at any time t is determined from a knowledge of the population of carriers in both extended and localized states at all previous times $t'<t$. The system's response is characterized by the function $s_n(t)$, which describes the probability that an electron resides in state n for time interval t. The survival probability is factored into the product $s_n(t)=s_n^C(t)s_n^T(t)$, where $s_n^C(t)=\exp(-e_nt)$ and $s_n^T(t)=\exp(-\Sigma_m w_{nm}t)$ are the elemental probabilities of surviving thermal emission to the conduction band and tunneling transitions to localized states, respectively.

2. Configurational average

The problem to be addressed here is the tunneling interactions between localized states as a function of their positions and energies. A reasonable approach in this regard is to introduce a statistical technique. Here, we apply the configurational average around a given state n by integrating over all possible positions and energies of surrounding states m weighted by the probability $P(\mathbf{r}_1,\ldots,\mathbf{r}_M;\varepsilon_1,\ldots,\varepsilon_M)$ of their occurrence. The method is similar to that used by Stoddart, Vardeny, and Tauc[7] for analyzing low-temperature photoinduced absorption in a-Si:H.

The corresponding operation is symbolically written as

$$\langle\,\rangle_{\{m\}}=\int d^3\mathbf{r}_1\cdots d^3\mathbf{r}_M d\varepsilon_1\cdots d\varepsilon_M P(\mathbf{r}_1,\ldots,\mathbf{r}_M;\varepsilon_1,\ldots,\varepsilon_M). \tag{3}$$

An enormous number of states M in volume V, over which the space integral in the above expression is performed, are of interest in the present argument. The configurational average around a specific state depends only on its energy for a spatially homogenous distribution. If we assume the absence of correlation between the arrangement of states, the probability P factors into M identical probabilities p as

$$P(\mathbf{r}_1,\ldots,\mathbf{r}_M;\varepsilon_1,\ldots,\varepsilon_M)=\prod_{m=1}^{M}p(\mathbf{r}_m,\varepsilon_m). \tag{4}$$

Under these conditions, the configurational average prescribed by Eq. (3) is then a straightforward calculation giving the survival probability against tunneling transitions as

$$\langle s_n^T(t)\rangle_{\{m\}}=\left(\int d^3\mathbf{r}_m d\varepsilon_m p(\mathbf{r}_m,\varepsilon_m)\exp(-w_{nm}t)\right)^M. \tag{5}$$

In this expression, the label m is used to merely denote an arbitrary final state. For a random distribution, the probability $p(\mathbf{r},\varepsilon)$ is actually position independent and simply represented as the density of localized states $D(\varepsilon)$ divided by the number M. In the limit as V becomes infinite, while the density $M/V=\int d\varepsilon\,D(\varepsilon)$ remains finite, we obtain

$$\langle s_n^T(t)\rangle_{\{m\}}\to S^T(\varepsilon_n,t)=\exp\left(-\int d\varepsilon_m D(\varepsilon_m)\int d^3\mathbf{r}_m\times\{1-\exp(-w_{nm}t)\}\right), \tag{6}$$

where the well-known formula $\lim_{M\to\infty}(1-x/M)^M=\exp(-x)$ has been used. A similar statistical treatment of the integrand in the second term on the right-hand side of Eq. (2) leads to the expression

$$\begin{aligned}\left\langle\sum_m f_m(t')w_{mn}s_n^T(t-t')\right\rangle_{\{m\}}&=\sum_m\langle f_m(t')w_{mn}\exp[-w_{nm}(t-t')]\rangle_m\\&\quad\times\left\langle\exp\left(-\sum_{m'\neq m}w_{nm'}(t-t')\right)\right\rangle_{\{m'\neq m\}}\\&\to S^T(\varepsilon_n,t-t')\int d\varepsilon_m D(\varepsilon_m)f(\varepsilon_m,t')\int d^3\mathbf{r}_m w_{mn}\\&\quad\times\exp[-w_{nm}(t-t')].\end{aligned}$$

The use of detailed balance between w_{mn} and w_{nm} rearranges the above result into the form

$$\begin{aligned}\left\langle\sum_m f_m(t')w_{mn}s_n^T(t-t')\right\rangle_{\{m\}}&\to S^T(\varepsilon_n,t-t')\int d\varepsilon_m D(\varepsilon_m)f(\varepsilon_m,t')\\&\quad\times\exp\left(-\frac{\varepsilon_n-\varepsilon_m}{kT}\right)\frac{d}{dt}\int d^3\mathbf{r}_m\{1-\exp[-w_{nm}(t-t')]\},\end{aligned} \tag{7}$$

which contains the same space integral as in Eq. (6). A different averaging procedure was applied in our previous analysis,[9] namely, the quantity $\langle\exp(-\Sigma_m w_{nm}t)\rangle_{\{m\}}$ is treated

approximately as $\exp(-\Sigma_m \langle w_{nm} \rangle_m t)$. In Appendix B, results following from these different averaging procedures are compared.

3. Formulation for discrete levels

The arguments given above make use of the continuous density of states in the statistical treatment. However, in order to obtain a concise expression and to facilitate a numerical computation, details of which will be presented in Sec. III, the formulation in terms of a discrete density of states $D(\varepsilon) = \Sigma_j N_j \delta(\varepsilon - \varepsilon_j)$ is preferred. There is no loss in generality because the continuum limit may be restored by considering an infinitesimal level spacing.

For the distribution of discrete levels, the averaged survival probability against tunneling transitions can be written for a level i of energy ε_i as

$$S_i^T(t) = \exp\left(-\sum_{j \neq i} N_j V_{ij}(t) \right). \tag{8}$$

By definition, $N_j V_{ij}(t)$ represents the average number of sites of level j to which an electron trapped at level i is transferable via tunneling within time t. The contribution due to an isoenergetic transition $j = i$ is removed from the summation since it does not affect the level occupation. The critical volume $V_{ij}(t)$ is given explicitly by

$$V_{ij}(t) = \int_0^\infty dr\, 4\pi r^2 \{1 - \exp[-w_{ij}(r)t]\}, \tag{9}$$

where $w_{ij}(r) = \nu_{ij} \exp(-2r/a)$ is the tunneling transition rate and $\nu_{ij} = \nu(\varepsilon_j - \varepsilon_i)$ is the energy-dependent prefactor. The overall survival probability is expressed as $S_i(t) = S_i^C(t) S_i^T(t)$, where $S_i^C(t) = \exp(-e_i t)$ with $e_i = e(\varepsilon_i)$. It is convenient to introduce the definition

$$C_{ji}(t) = \exp\left(-\frac{\varepsilon_i - \varepsilon_j}{kT} \right) \frac{d}{dt} V_{ij}(t). \tag{10}$$

It can be understood from the derivation of Eq. (7) that $C_{ji}(t)$ describes the probability that an electron trapped at level j makes a transition to level i and does not return to level j in time interval t. With these notations, the nonequilibrium occupancy originally given by Eq. (2) becomes

$$f_i(t) = \int_{-\infty}^t dt' n_c(t') C S_i(t - t') + \sum_{j \neq i} N_j \int_{-\infty}^t dt' f_j(t') C_{ji}(t - t') S_i(t - t'). \tag{11}$$

As explicitly shown by its series expansion,

$$\begin{aligned} f_i(t) = & \int_{-\infty}^t dt' n_c(t') C S_i(t - t') \\ & + \int_{-\infty}^t dt' \int_{-\infty}^{t'} dt'' n_c(t'') C \sum_{j \neq i} S_j(t' - t'') N_j \\ & \times C_{ji}(t - t') S_i(t - t') \\ & + \int_{-\infty}^t dt' \int_{-\infty}^{t'} dt'' \int_{-\infty}^{t''} dt''' n_c(t''') \\ & \times C \sum_{j \neq i} \sum_{k \neq j} S_k(t'' - t''') N_k C_{kj}(t' - t'') S_j(t' - t'') \\ & \times N_j C_{ji}(t - t') S_i(t - t') + \cdots, \end{aligned}$$

Equation (11) accounts for a sequence of tunneling events to infinite times.

Before closing this section, it may be appropriate to evaluate analytically the volume $V_{ij}(t)$, which crucially characterizes the tunneling interactions between localized states. A rough assessment, expressed by

$$V_{ij}(t) = \frac{\pi a^3}{6} [\ln(\nu_{ij} t)]^3 \theta(\nu_{ij} t - 1), \tag{12}$$

is obtained from the approximation that $\exp(-e^{-x}) \approx \theta(x)$. Note that a time-dependent critical transfer radius $r_{ij}(t)$, determined from the condition that $w_{ij}(r_{ij}(t))t = 1$ for $\nu_{ij} t > 1$, directly defines a sphere with volume $V_{ij}(t) = 4\pi[r_{ij}(t)]^3/3$, which exactly coincides with Eq. (12). A similar expression is found in some literature[8,12,13] dealing with tunneling events in an ensemble of randomly positioned sites. It is, however, evident that the step-function approximation does not hold with sufficient accuracy near $x = 0$. A more rigorous treatment based on the improved approximation,[7] $\exp(-e^{-x}) \cong \theta(x)(1 - e^{-x})$, leads to

$$V_{ij}(t) = \pi a^3 \times \begin{cases} \nu_{ij} t, & \nu_{ij} t < 1, \\ \displaystyle\sum_{k=0}^{3} \frac{[\ln(\nu_{ij} t)]^k}{k!}, & \nu_{ij} t > 1 \end{cases}. \tag{13}$$

This illustrates that the tunneling volume $V_{ij}(t)$ increases linearly with time up to $t = 1/\nu_{ij}$ when its time dependence smoothly turns logarithmic. At long times such that $\ln(\nu_{ij} t) \gg 1$, Eqs. (12) and (13) become equivalent.

B. Recombination

In this section, we generalize the theory by considering recombination events. Recombination can occur by the capture of band carriers into deep states occupied by carriers of the opposite type, as well as by the tunneling transitions between electrons and holes trapped in the localized states. Both processes are described below within the framework of monomolecular recombination mechanism.[14]

The tunneling recombination process is formally included in the rate equation (1), by appending a proper term containing the transition rate to recombination centers. In the monomolecular case, we may write

$$\frac{d}{dt}f_n(t)=n_c(t)C-f_n(t)e_n + \sum_m f_m(t)w_{mn}-f_n(t)\left(\sum_m w_{nm}+\sum_l w_{nl}\right), \tag{14}$$

where l indexes recombination centers and distinguishes them from states m acting as traps. The additional transition channels provided by recombination decrease the total survival probability $s_n(t)=s_n^C(t)s_n^T(t)s_n^R(t)$, where the multiplicative factor $s_n^R(t)=\exp(-\Sigma_l w_{nl}t)$ is the probability that an electron trapped in state n survives recombination transitions during time t. It is reasonable to assume that the recombination centers are randomly distributed in space. In that case, the configurational average introduced in Sec. II A applies similarly for the probability $s_n^R(t)$. Since all the recombination transitions are downward in energy, we have in the infinite volume limit,

$$S^R(t)=\exp[-N_R V_0(t)]. \tag{15}$$

Here, N_R is the density of recombination centers and $V_0(t)$ is the relevant interaction volume, which is given by Eq. (13) with ν_{ij} replaced by ν_0 and is energy independent. In the discrete-level case, the averaged survival probability against all release events is written in product form

$$S_i(t)=S_i^C(t)S_i^T(t)S^R(t), \tag{16}$$

as prescribed by the statistical independence of each factor. In the presence of tunneling recombination, Eq. (11) describes the nonequilibrium occupation while the survival probability $S_i(t)$ involved in it is given by Eq. (16).

In order to obtain a closed-form solution to the problem, we next address the continuity equation for all the electrons. This is represented under uniform photoexcitation as

$$\frac{d}{dt}\left(n_c(t)+\frac{1}{V}\sum_n f_n(t)\right) = G(t)-n_c(t)CN_R-\frac{1}{V}\sum_n f_n(t)\sum_l w_{nl}, \tag{17}$$

where $G(t)$ denotes the generation rate. The recombination rate consists of two terms. The first term $n_c(t)CN_R$ accounts for the capture of band electrons into the recombination centers. The strategy for dealing with the second term $V^{-1}\Sigma_n f_n(t)\Sigma_l w_{nl}$, which describes tunneling recombination, proceeds as before. The first step involves independent configurational averages over the associated states m and l,

$$\left\langle f_n(t)\sum_l w_{nl}\right\rangle_{\{m,l\}} = \int_{-\infty}^{t} dt' n_c(t')Cs_n^C(t-t')\langle s_n^T(t-t')\rangle_{\{m\}} \times\left\langle s_n^R(t-t')\sum_l w_{nl}\right\rangle_{\{l\}} + \int_{-\infty}^{t} dt' s_n^C(t-t') \times\left\langle\sum_m f_m(t')w_{mn}s_n^T(t-t')\right\rangle_{\{m\}}\left\langle s_n^R(t-t')\sum_l w_{nl}\right\rangle_{\{l\}}.$$

It is easily found that the recombination factor reduces to $\langle s_n^R(t)\Sigma_l w_{nl}\rangle_{\{l\}}=-d\langle s_n^R(t)\rangle_{\{l\}}/dt$, corresponding to $-dS^R(t)/dt$ in the infinite volume limit. In view of this relationship, we introduce the time-dependent rate,

$$Q_i(t)=-S_i^C(t)S_i^T(t)\frac{d}{dt}S^R(t)=S_i(t)N_R\frac{d}{dt}V_0(t), \tag{18}$$

which represents the decay of electron population at level i due to losses by recombination transitions. Consequently, the continuity equation is formulated as

$$\frac{d}{dt}\left(n_c(t)+\sum_i N_i f_i(t)\right)=G(t)-R(t), \tag{19}$$

with the configurationally averaged recombination rate expressed as

$$R(t)=n_c(t)CN_R+\sum_i N_i r_i(t), \tag{20}$$

where the function $r_i(t)$, given by the right-hand side of Eq. (11) with replacing $S_i(t)$ by $Q_i(t)$, accounts for the recombination processes via multiple tunneling.

C. Fourier transform

A more tractable form of the integrals in Eqs. (11) and (20) is obtained via Fourier transformation, $\tilde{f}(\omega)=\mathcal{F}[f(t)]=\int_{-\infty}^{\infty}dt\, f(t)\exp(-i\omega t)$. In terms of linear response theory, it follows that this familiar technique provides a direct connection to MPC. This formal statement is verified by noting that the Fourier-transformed configurational average $\mathcal{F}[\langle\cdots\rangle]$ is identical with the configurationally averaged Fourier transform $\langle\mathcal{F}[\cdots]\rangle$. In this sense, the operation of configurational averaging originally carried out in the time domain is preserved in the frequency domain.

For convenience, we define the following transfer functions:

$$\tilde{\alpha}_i(\omega)=\mathcal{F}[CN_iS_i(t)\theta(t)],$$

$$\tilde{\beta}_{ji}(\omega)=\mathcal{F}[C_{ji}(t)N_iS_i(t)\theta(t)],$$

$$\tilde{\phi}(\omega)=\mathcal{F}\left[\sum_i CN_iQ_i(t)\theta(t)\right],$$

$$\tilde{\varphi}_j(\omega)=\mathcal{F}\left[\sum_{i\neq j} C_{ji}(t)N_iQ_i(t)\theta(t)\right].$$

The frequency-domain equations are simply represented in terms of these functions as

$$\tilde{n}_i(\omega)=\tilde{n}_c(\omega)\tilde{\alpha}_i(\omega)+\sum_{j\neq i}\tilde{n}_j(\omega)\tilde{\beta}_{ji}(\omega), \tag{21}$$

$$i\omega\tilde{N}(\omega)=\tilde{G}(\omega)-\tilde{R}(\omega), \tag{22}$$

$$\tilde{R}(\omega)=\tilde{n}_c(\omega)[CN_R+\tilde{\phi}(\omega)]+\sum_j \tilde{n}_j(\omega)\tilde{\varphi}_j(\omega), \tag{23}$$

with respect to the concentrations of band electrons $\tilde{n}_c(\omega)$ and trapped electrons $\tilde{n}_i(\omega)=N_i\tilde{f}_i(\omega)$, as well as their total concentration $\tilde{N}(\omega)=\tilde{n}_c(\omega)+\Sigma_i\tilde{n}_i(\omega)$. Equations (21)–(23) correspond to the time-domain equations (11), (19), and (20), respectively. There is one frequency-domain rate equation (21) for each energy level. Its matrix form,

$$\begin{pmatrix} 1/\tilde{\alpha}_1 & -\tilde{\beta}_{21}/\tilde{\alpha}_1\cdots & -\tilde{\beta}_{i1}/\tilde{\alpha}_1\cdots & -\tilde{\beta}_{j1}/\tilde{\alpha}_1\cdots \\ -\tilde{\beta}_{12}/\tilde{\alpha}_2 & 1/\tilde{\alpha}_2 & \cdots -\tilde{\beta}_{i2}/\tilde{\alpha}_2\cdots & -\tilde{\beta}_{j2}/\tilde{\alpha}_2\cdots \\ \vdots & \vdots & \ddots \quad \vdots & \vdots \\ -\tilde{\beta}_{1i}/\tilde{\alpha}_i & -\tilde{\beta}_{2i}/\tilde{\alpha}_i\cdots & 1/\tilde{\alpha}_i \quad \cdots & -\tilde{\beta}_{ji}/\tilde{\alpha}_i\cdots \\ \vdots & \vdots & \vdots \quad \ddots & \vdots \\ -\tilde{\beta}_{1j}/\tilde{\alpha}_j & -\tilde{\beta}_{2j}/\tilde{\alpha}_j\cdots & -\tilde{\beta}_{ij}/\tilde{\alpha}_j\cdots & 1/\tilde{\alpha}_j \quad \cdots \\ \vdots & \vdots & \vdots & \vdots \quad \ddots \end{pmatrix}$$

$$\times\begin{pmatrix} \tilde{n}_1/\tilde{n}_c \\ \tilde{n}_2/\tilde{n}_c \\ \vdots \\ \tilde{n}_i/\tilde{n}_c \\ \vdots \\ \tilde{n}_j/\tilde{n}_c \\ \vdots \end{pmatrix}=\begin{pmatrix} 1 \\ 1 \\ \vdots \\ 1 \\ \vdots \\ 1 \\ \vdots \end{pmatrix},$$

explains that the inverse of the matrix composed of transfer functions forms the solution for the population ratios $\tilde{n}_i(\omega)/\tilde{n}_c(\omega)$.

In our previous study, the drift mobility $\mu(\omega)$ and the average lifetime $\tau(\omega)$ for all the charge carriers involved in transport were introduced in order to formulate MPC in a phenomenological and thereby model-independent manner.[9] Here, we briefly outline the theoretical expressions in order to relate them to the present considerations. These transport parameters are written in the notation of this article by $\mu(\omega)=\tilde{\sigma}(\omega)/q\tilde{N}(\omega)$ and $\tau(\omega)=\tilde{N}(\omega)/\tilde{R}(\omega)$, respectively, where $\tilde{\sigma}(\omega)$ denotes the Fourier-transformed photoconductivity and q the unit electronic charge. For any spatially homogeneous illumination, the comprehensive relationship

$$\tilde{\sigma}(\omega)=q\mu(\omega)\frac{\tilde{G}(\omega)\tau(\omega)}{1+i\omega\tau(\omega)}, \tag{24}$$

follows from the continuity equation (22). This defines an important experimental parameter

$$\mu_{\mathrm{MPC}}\equiv\frac{i\omega\tilde{\sigma}(\omega)}{q\tilde{G}(\omega)}=\mu(\omega)\frac{i\omega\tau(\omega)}{1+i\omega\tau(\omega)}, \tag{25}$$

which coincides with the true drift mobility $\mu(\omega)$ in the high-frequency regime where the condition that $\omega|\tau(\omega)|\gg 1$ is met. On the other hand, in the low-frequency regime where $\omega|\tau(\omega)|\ll 1$, μ_{MPC} is reduced to $i\omega\mu(\omega)\tau(\omega)$.

In the context of the present theory, the average lifetime is given straightforwardly from Eq. (23) by

$$\tau(\omega)=\frac{\tilde{N}(\omega)}{\tilde{n}_c(\omega)[CN_R+\tilde{\phi}(\omega)]+\sum_j\tilde{n}_j(\omega)\tilde{\varphi}_j(\omega)}. \tag{26}$$

It is widely accepted for a-Si:H that electron transport via extended states dominates photoconduction at sufficiently high temperatures and thereby $\tilde{\sigma}(\omega)=q\mu_c\tilde{n}_c(\omega)$ where μ_c is the band electron mobility. Then, the high-temperature drift mobility is simply written as

$$\mu(\omega)=\mu_c\frac{\tilde{n}_c(\omega)}{\tilde{N}(\omega)}, \tag{27}$$

which is directly determined by solving Eq. (21). The theoretical considerations in Appendix C are concerned with the contribution due to hopping transport through localized states, and prove quantitatively that Eq. (27) has practical validity over a wide temperature range.

D. Steady state

The steady-state formula for nonequilibrium occupation is derived from the time average of the original equation (11) or equivalently from the low-frequency limit of the transformed equation (21). The result is

$$\overline{f_i}=\overline{n_c}C\int_0^\infty dt\,S_i(t)+\sum_{j\neq i}N_j\overline{f_j}\int_0^\infty dt\,C_{ji}(t)S_i(t), \tag{28}$$

where an overbar denotes the steady state. In order to analyze the steady-state occupancy $\overline{f_i}$, it is helpful to consider the probability per unit time of electron release $P_i(t)\equiv -dS_i(t)/dt$, normalized as

$$\begin{aligned}1&=\int_0^\infty dt\,P_i(t)\\&=e_i\int_0^\infty dt\,S_i(t)+\sum_{j\neq i}N_j\int_0^\infty dt\,S_i(t)\frac{d}{dt}V_{ij}(t)\\&\quad+\int_0^\infty dt\,Q_i(t).\end{aligned} \tag{29}$$

Using the tunneling capture coefficient $C_{ji}(t) = (e_j/e_i)dV_{ij}(t)/dt$, we can rewrite Eq. (29) as

$$\frac{\overline{n_c C}}{e_i}\left(1-\int_0^\infty dt\, Q_i(t)\right) = \overline{n}_c C\int_0^\infty dt\, S_i(t)+\sum_{j\neq i} N_j \frac{\overline{n}_c C}{e_j}\int_0^\infty dt\, C_{ji}(t)S_i(t). \tag{30}$$

A comparison of Eqs. (28) and (30) shows that when the dimensionless quantity $\int_0^\infty dt\, Q_i(t)$ is much smaller than unity, the steady-state occupancy has a Boltzmann form

$$\overline{f}_i = \frac{\overline{n}_c C}{e_i} = \exp\left(-\frac{\varepsilon_i-\varepsilon_{fn}}{kT}\right), \tag{31}$$

where $\varepsilon_{fn}=\varepsilon_c - kT\ln(N_c/\overline{n_c})$ is the quasi-Fermi-level for band electrons. This result is naturally understood as arising from the detailed balance relations imposed on all the transitions other than recombination.

The mathematical manipulation applied above is made physically transparent by directly considering the configurational average in the steady state. The electron release channels from a certain initial state *n* include thermal emission to the conduction band, and tunneling transitions to the trap states *m* as well as to the recombination centers *l*. The efficiencies of the relevant events are given by

$$\chi_n^C = \frac{e_n}{e_n+\sum_m w_{nm}+\sum_l w_{nl}},$$

$$\chi_n^T = \frac{\sum_m w_{nm}}{e_n+\sum_m w_{nm}+\sum_l w_{nl}},$$

$$\chi_n^R = \frac{\sum_l w_{nl}}{e_n+\sum_m w_{nm}+\sum_l w_{nl}},$$

respectively, where $\chi_n^C+\chi_n^T+\chi_n^R=1$. Because correlation between the numerator and denominator in these expressions is generally important, it is not sufficient to average them separately. The trick to managing this problem involves the integral form. For instance, the configurational averaging of the efficiency χ_n^R proceeds as follows:

$$\begin{aligned}\langle\chi_n^R\rangle_{\{m,l\}} &= \int_0^\infty dt\left\langle \sum_l w_{nl} \times\exp\left[-\left(e_n+\sum_m w_{nm}+\sum_l w_{nl}\right)t\right]\right\rangle_{\{m,l\}} \\ &= \int_0^\infty dt\exp(-e_n t) \times\left\langle \exp\left(-\sum_m w_{nm}t\right)\right\rangle_{\{m\}} \times\left\langle \exp\left(-\sum_l w_{nl}t\right)\sum_l w_{nl}\right\rangle_{\{l\}} \\ &= -\int_0^\infty dt s_n^C(t)\langle s_n^T(t)\rangle_{\{m\}}\frac{d}{dt}\langle s_n^R(t)\rangle_{\{l\}}.\end{aligned}$$

The same treatment can be applied to the other release efficiencies. In the infinite volume limit, the results are written for a level *i* as

$$\chi_i^C = e_i\int_0^\infty dt S_i(t), \tag{32a}$$

$$\chi_i^T = \sum_{j\neq i} N_j\int_0^\infty dt S_i(t)\frac{d}{dt}V_{ij}(t), \tag{32b}$$

$$\chi_i^R = \int_0^\infty dt Q_i(t), \tag{32c}$$

subject to the sum rule $\chi_i^C+\chi_i^T+\chi_i^R=1$. This is exactly what is stated by Eq. (29). The steady-state occupancy is averaged in a similar way. Thus,

$$\begin{aligned}\langle\overline{f}_n\rangle_{\{m,l\}} &= \left\langle\frac{\overline{n}_c C+\sum_m \overline{f}_m w_{mn}}{e_n+\sum_m w_{nm}+\sum_l w_{nl}}\right\rangle_{\{m,l\}} \\ &= \overline{n}_c C\int_0^\infty dt\, s_n^C(t)\langle s_n^T(t)\rangle_{\{m\}}\langle s_n^R(t)\rangle_{\{l\}} \\ &\quad + \int_0^\infty dt\, s_n^C(t)\left\langle\sum_m \overline{f}_m w_{mn}s_n^T(t)\right\rangle_{\{m\}}\langle s_n^R(t)\rangle_{\{l\}},\end{aligned}$$

which leads to $\overline{f}_i$ given by Eq. (28). Likewise, we can obtain the averaged efficiencies of capturing band electrons ρ_n^C and trapped electrons ρ_n^T defined by

$$\langle\rho_n^C\rangle_{\{m,l\}} = \left\langle\frac{\overline{n}_c C}{\overline{n}_c C+\sum_m \overline{f}_m w_{mn}}\right\rangle_{\{m,l\}},$$

$$\langle\rho_n^T\rangle_{\{m,l\}} = \left\langle\frac{\sum_m \overline{f}_m w_{mn}}{\overline{n}_c C+\sum_m \overline{f}_m w_{mn}}\right\rangle_{\{m,l\}},$$

Relating the denominator in these expressions to $\overline{f}_n$, we calculate that

$$\rho_i^C = \frac{\overline{n}_c C}{\overline{f}_i} \int_0^\infty dt\, S_i(t), \tag{33a}$$

$$\rho_i^T = \frac{1}{\overline{f}_i} \sum_{j \neq i} N_j \overline{f}_j \int_0^\infty dt\, C_{ji}(t) S_i(t). \tag{33b}$$

The sum rule $\rho_i^C + \rho_i^T = 1$ and the identities $\chi_i^C = \rho_i^C$ and $\chi_i^T = \rho_i^T$ for $\chi_i^R \ll 1$ are readily confirmed from Eqs. (28) and (31), respectively.

Finally, we provide the steady-state recombination rate,

$$\overline{R} = \overline{n}_c C N_R + \overline{n}_c C \sum_i \int_0^\infty dt\, N_i Q_i(t) + \sum_j \overline{n}_j \sum_{i \neq j} \int_0^\infty dt\, C_{ji}(t) N_i Q_i(t), \tag{34}$$

derived directly from the Fourier transform, Eq. (23), with $\omega = 0$. The same result is reached from averaging the steady-state version of the recombination rate contained in Eq. (17). The proportion of the number of active recombination channels, either by the direct capture of band electrons η^C or the tunneling transfer of trapped electrons η^T, is determined from this expression to be

$$\eta^C = \frac{\overline{n}_c C N_R}{\overline{R}}, \tag{35a}$$

$$\eta^T = \frac{1}{\overline{R}} \left(\overline{n}_c C \sum_i \int_0^\infty dt\, N_i Q_i(t) + \sum_j \overline{n}_j \sum_{i \neq j} \int_0^\infty dt\, C_{ji}(t) N_i Q_i(t) \right). \tag{35b}$$

where $\eta^C + \eta^T = 1$. The efficiency η^C determines the effective capture coefficient $C_{\text{eff}} = C/\eta^C$ for the recombination centers such that the total recombination rate $\overline{R}$ is the same as it would be if only the band electrons were captured but the recombination centers had the capture coefficient C_{eff}. The enhancement factor $1/\eta^C$ obtained here is distinct from those evaluated in previous analyses[15,16] where multiple tunneling transitions experienced by an electron are completely ignored.

III. NUMERICAL ANALYSIS AND DISCUSSION

This section investigates thermalization and recombination in the presence of tunneling transitions by numerical calculation and compares the theoretical results with experiment. The calculation incorporates the density of states, which has been introduced to describe the conduction-band tail in a-Si:H,[9,17,18]

$$D(\varepsilon) = D_c \times \begin{cases} 1 - \dfrac{\varepsilon_c - \varepsilon}{\Delta}, & \varepsilon_c - \varepsilon < \Delta - kT_c, \\ \dfrac{kT_c}{\Delta} \exp\left(- \dfrac{\varepsilon_c - \varepsilon - \Delta + kT_c}{kT_c} \right), & \varepsilon_c - \varepsilon > \Delta - kT_c. \end{cases} \tag{36}$$

This distribution decreases linearly from the conduction-band edge ε_c, and thereafter decreases exponentially into the gap. A linear distribution for the extended states extrapolated above ε_c gives the effective density of states $N_c = D_c kT(1 + kT/\Delta)$. The simulation represents the continuous distribution by a ladder of discrete levels $N_j = D(\varepsilon_j)\,\delta\varepsilon$. The energy spacing $\delta\varepsilon$ was normally set at 20 meV. It has been confirmed that applying $\delta\varepsilon$ less than this value does not alter the calculated result. Parameters used in the calculation are $D_c = 2 \times 10^{21}\,\text{cm}^{-3}\,\text{eV}^{-1}$, $\Delta = 0.1\,\text{eV}$, $T_c = 220\,\text{K}$, $C = 10^{-8}\,\text{cm}^3\,\text{s}^{-1}$, and $a = 1\,\text{nm}$. The value of the localization radius a is compatible with previous estimates[12,19] for band-tail electrons in a-Si:H. The same frequency prefactor $\nu_0 = N_c C$ for tunneling transitions, and thermal emissions was assumed for simplicity. This is reasonable in the case when tunneling transitions are nonradiative. The value chosen for the characteristic temperature T_c is based on agreement with the drift mobility experiments, which will be described in detail in Sec. III C. The Fourier transforms required for the frequency-domain analysis were computed with Gaussian weighting in order to improve convergence of the numerical integration. Care was taken to keep the resulting broadening in frequency domain negligibly small.

A. Thermalization in band-tail states

First, we investigate thermalization in band-tail states in the absence of recombination. Figure 1 displays survival

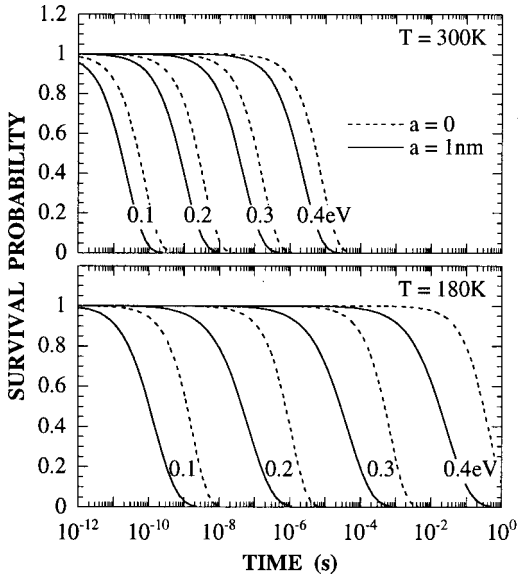

FIG. 1. Time evolution of survival probabilities $S_i(t)$ for various energies $\varepsilon_c - \varepsilon_i = 0.1$, 0.2, 0.3 and 0.4 eV in the absence of recombination. Dashed and full lines represent the results computed for localization radii $a = 0$ and 1 nm, respectively. The calculation is based on the density of states given by Eq. (36). The upper and lower figures correspond to $T = 300$ and 180 K, respectively.

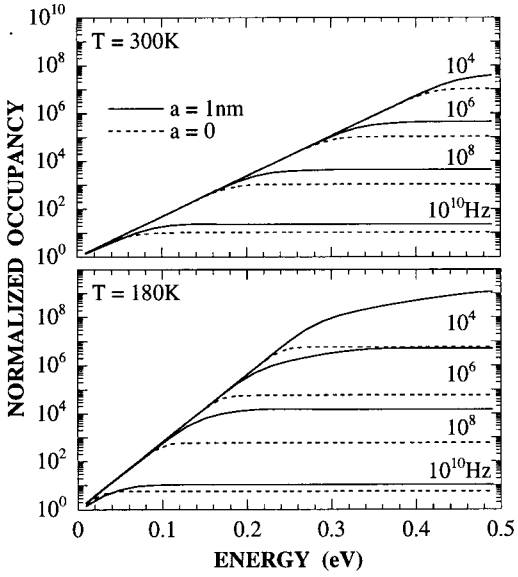

FIG. 2. Normalized occupation functions $|\tilde{f}_i(\omega)/\tilde{f}_c(\omega)|$ for various frequencies $\omega/2\pi = 10^4$, 10^6, 10^8, and 10^{10} Hz. Dashed and full lines represent the results computed for $a=0$ and 1 nm, respectively. The upper figure corresponds to $T=300$ K while the lower figure is for 180 K.

probability as a function of time. The dashed curves for $a=0$ correspond to the elemental survival probability $S_i^C(t)$ controlled only by the thermal emission rate e_i. The solid curves for $a=1$ nm represent the total survival probability $S_i(t)=S_i^C(t)S_i^T(t)$ including the contribution due to tunneling release. It is immediately apparent from this figure that even for room temperature, the survival probability decays considerably faster in the presence of tunneling transitions. The promotion of electron release becomes even more pronounced with decreasing temperature. From this observation one realizes that the effect of tunneling transitions is quite substantial and that the ordinary multiple trapping model does not adequately describe the band-tail electron dynamics. The figure also reveals that the tunneling releases are thermally activated, particularly for deep energy states, indicating a dominance of upward transitions. How the releases are divided between the upward and downward transitions is discussed analytically in Appendix A.

Figure 2 illustrates the absolute values of the Fourier-transformed occupancy $\tilde{f}_i(\omega)=\tilde{n}_i(\omega)/N_i$ as a function of energy, divided by the effective occupancy for conduction band $\tilde{f}_c(\omega)\equiv\tilde{n}_c(\omega)/N_c$. In the shallow-energy region the normalized occupation function obeys the Boltzmann distribution $\exp[(\varepsilon_c-\varepsilon_i)/kT]$, indicating that the relevant states are in quasithermal equilibrium with the conduction band. On the other hand, the nonequilibrium occupation appears in the deep-energy region where thermal contact with the conduction band cannot be established within a time scale of $1/\omega$. The thermalization energy that separates the equilibrium from nonequilibrium occupation descends in the gap with decreasing frequency. Simultaneously the deep nonequilibrium occupancy becomes more prominent. As temperature decreases, the thermalization energy shifts upward so that the

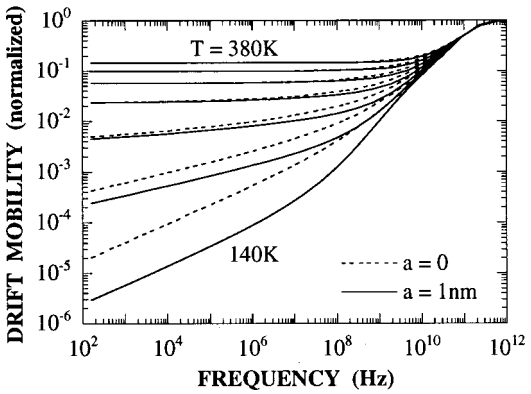

FIG. 3. Frequency dependence of the normalized drift mobility $|\mu(\omega)|/\mu_c$ for temperatures varied from $T=140$ to 380 K in 40-K steps. Dashed and full lines represent the results computed for $a=0$ and 1 nm, respectively.

energy range where the nonequilibrium occupancy occurs broadens. These qualitative features are commonly observed for both $a=0$ nm and $a=1$ nm, while the calculation clearly indicates that the tunneling interactions produce a deeply positioned thermalization energy as well as an increased deep nonequilibrium occupancy. The effects are enhanced at low temperatures. Note that the frequency-domain thermalization event addressed here corresponds to progressively deeper trapping in the time domain, which involves the effects of tunneling transitions as demonstrated by the survival probability plotted in Fig. 1. From additional calculations, we have observed that the frequency-dependent thermalization energy is represented to a good approximation by the energy at which the mean survival time, determined by the integration $\int_0^\infty dt\, S_i(t)$, coincides with $1/\omega$.

Figure 3 shows the frequency-resolved spectra of the drift-mobility amplitude $|\mu(\omega)|$, given by Eq. (27), computed for various temperatures. The drift-mobility behavior depicted in the figure is easily understood in terms of arguments based on the occupation function. At a certain temperature, the thermalization energy deepens with decreasing frequency, followed by the increasing population ratio of trapped electrons to band electrons and thereby the decreasing magnitude of drift mobility. As temperature decreases, the drift mobility observed at any fixed frequency is reduced due to a relative increase in population of trapped electrons. The tunneling interactions between band-tail states accelerate the thermalization process and lower the frequency-dependent drift mobility. It should be noted that the drift mobility in the low-frequency limit, as the occupation function approaches the Boltzmann distribution over the whole energy range, is independent of the presence or otherwise of intra-band-tail transitions. The above discussions do not reference phases of the associated quantities. As expected, the band-tail occupancy $\tilde{f}_i(\omega)$ is in phase with $\tilde{f}_c(\omega)$ in the equilibrium region as well as out of phase with $\tilde{f}_c(\omega)$ in the nonequilibrium region. Accordingly, the drift-mobility phase varies with frequency and goes to zero when the frequency becomes low enough for all the band-tail states to reach equilibrium with the conduction band. The phase graphs are

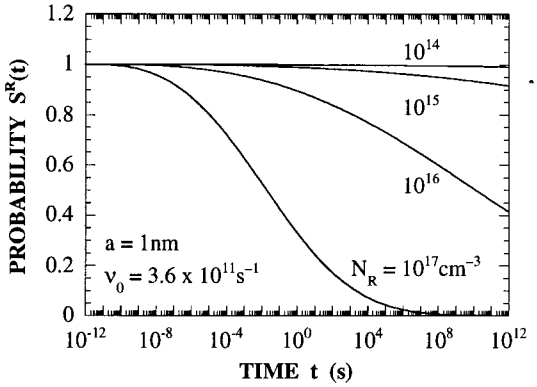

FIG. 4. Survival probabilities against recombination transitions $S^R(t)$ as a function of time for various densities of recombination centers $N_R = 10^{14}$, 10^{15}, 10^{16}, and $10^{17}\,\mathrm{cm}^{-3}$. The calculation assumes $\nu_0 = 3.6 \times 10^{11}\,\mathrm{s}^{-1}$ for $T = 180\,\mathrm{K}$.

not presented here. They are not necessarily needed in order to gain a fundamental understanding of results of the present experiments, which only concern the drift-mobility amplitude.

B. Recombination and deep trapping

This section shows how the results given in the preceding section are modified by the inclusion of recombination events. Since the recombination centers that N_R references may be somewhat vague, we specify them from a practical point of view before giving the quantitative analysis. In *a*-Si:H, the midgap defect states originating from Si dangling bonds play a significant role in recombination. For a high-quality intrinsic material, the defect density is not more than $10^{16}\,\mathrm{cm}^{-3}$. The other possible recombination sites are nonequilibrium holes captured in the valence-band tail, which make a dominant contribution to recombination at a low temperature. The measured density of band-tail holes[19,20] is at most $10^{17}\,\mathrm{cm}^{-3}$. Based on these observations, only values of N_R lower than $10^{17}\,\mathrm{cm}^{-3}$ are considered in the following arguments. In addition, the monomolecular recombination centers must satisfy the constraint that N_R remains constant in time. This can be fulfilled experimentally with sufficiently strong background illumination. In this case, the linearized theory is valid in the small-signal regime where the behavior of supplemental photocarriers is considered. Unless either the bias illumination is extremely strong or the temperature is extremely low, state filling is thought to be negligible for the conduction-band tail with the density of states decreasing steeply into the gap.

The survival probability against recombination transitions $S^R(t)$ strongly depends on the density of recombination centers, as illustrated in Fig. 4. This behavior can be quantified by the characteristic decay time, which is roughly given by $\exp[(6/\pi a^3 N_R)^{1/3}]/\nu_0$, for $N_R \ll 1/\pi a^3 \cong 3 \times 10^{20}\,\mathrm{cm}^{-3}$, from Eq. (15), and is slightly affected by variations in temperature through the frequency prefactor ν_0. The overall survival probability for band-tail electrons is reduced uniformly in energy by the multiplicative factor $S^R(t)$. In comparison

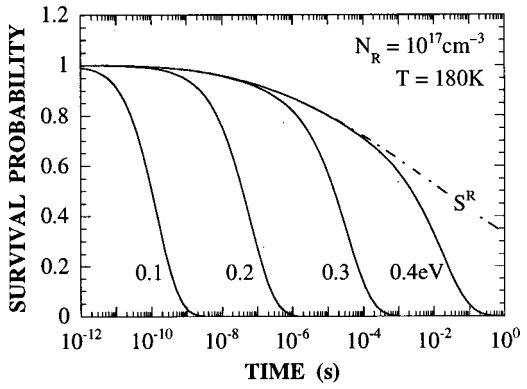

FIG. 5. Time evolution of survival probabilities $S_i(t)$ for different energies at $T = 180\,\mathrm{K}$ in the presence of recombination centers with $N_R = 10^{17}\,\mathrm{cm}^{-3}$. The chain-dotted line represents the function $S^R(t)$ plotted in Fig. 4.

with theoretical plots displayed in Fig. 1, it appears that the additional release yields a larger effect for lower temperatures when the probability $S_i^C(t)S_i^T(t)$ tends to decay slowly. Figure 5 demonstrates the influence of recombination transitions. The total survival probability $S_i(t) = S_i^C(t)S_i^T(t)S^R(t)$ calculated for $T = 180\,\mathrm{K}$ and $N_R = 10^{17}\,\mathrm{cm}^{-3}$ is shown in that figure.

Figure 6 presents the frequency dependence of the drift mobility and the average lifetime calculated at $T = 180\,\mathrm{K}$ for various densities of recombination centers. The calculation is based on Eqs. (21)–(23), which take into account the tunneling recombination of band-tail electrons in addition to the direct recombination of band electrons. It can be seen in the figure that the drift mobility increases only a little at low frequency in the presence of recombination even for $N_R = 10^{17}\,\mathrm{cm}^{-3}$. In terms of Eq. (21), it follows that the drift

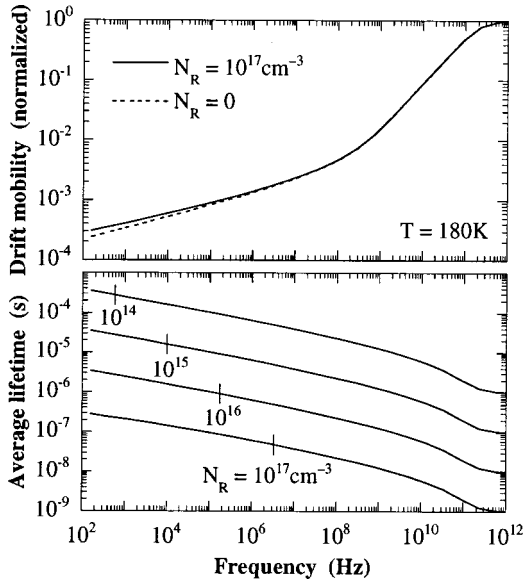

FIG. 6. Frequency dependence of the normalized drift mobility $|\mu(\omega)|/\mu_c$ and average lifetime $|\tau(\omega)|$ computed at $T = 180\,\mathrm{K}$ for various values of N_R. The vertical bar inserted in the lifetime plot indicates the frequency position at which $\omega|\tau(\omega)| = 1$.

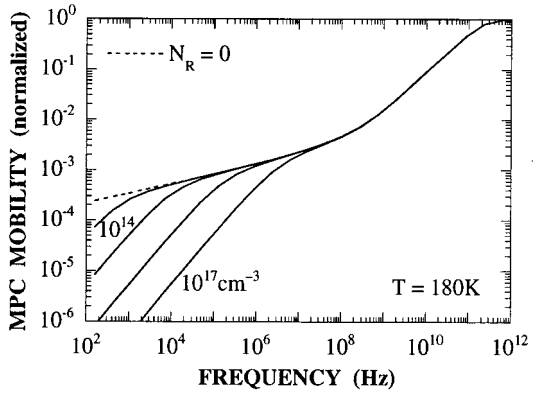

FIG. 7. Frequency dependence of the normalized MPC mobility $|\mu_{\mathrm{MPC}}|/\mu_c$ calculated at $T=180\,\mathrm{K}$ for various values of N_R.

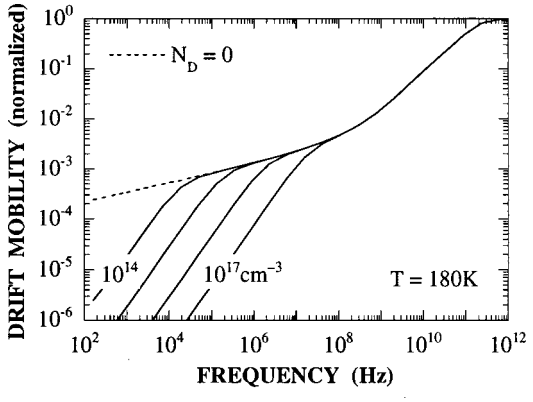

FIG. 8. Frequency dependence of the normalized drift mobility $|\mu(\omega)|/\mu_c$ calculated at $T=180\,\mathrm{K}$ for various values of N_D.

mobility is determined independently of the direct recombination of band electrons. Eventually, the increase of drift mobility is solely associated with loss of trapped electrons by tunneling recombination. In contrast to the drift-mobility behavior, the average lifetime is greatly affected by variations in N_R. The figure illustrates that the magnitude of the lifetime is almost inversely proportional to N_R. It is understood from inspecting Eq. (26) that this relation is characteristic of relatively low densities of recombination centers. The recombination processes involved are not evaluated directly from the average lifetime since it also correlates with the population ratio. The quantitative evaluation will be deferred until the steady-state analysis.

An experimentally accessible quantity in this work is the MPC mobility μ_{MPC}. The results of calculating this quantity by Eq. (25) are summarized in Fig. 7. Simulated spectra exhibit two branches separated by a knee. As expected, the spectrum in the high-frequency branch is not affected by recombination and exactly coincides with the drift mobility $\mu(\omega)$ controlled by thermalization in the band tail. The frequency at which the knee appears is determined by the condition that $\omega|\tau(\omega)|=1$. This can be confirmed by comparison with the lifetime plots in Fig. 6, where the corresponding frequencies are indicated by vertical bars. Similar observations were obtained for various temperatures.

The preceding discussions suppose that the deep-energy states, referred to as the recombination centers, are populated with background nonequilibrium carriers. When the illumination level is low enough or the temperature is high enough, the occupation of the valence-band tail almost stays in the dark equilibrium, and the midgap defect states are brought into play as trap centers rather than recombination centers. In this study, a deep trapping effect such as this has been simulated by a single level of energy $\varepsilon_c-0.6\,\mathrm{eV}$ appended to the band-tail levels. Note that the present theory does not consider any isoenergetic transitions. Hence, an exclusion of tunneling exists between defect states, as one might expect from their small wave-function overlap. The results calculated at $T=180\,\mathrm{K}$ for the deep-level densities ranging from $N_D=10^{14}$ to $10^{17}\,\mathrm{cm}^{-3}$ are summarized in Fig. 8. The drift-mobility spectra, $\mu(\omega)$, identical with μ_{MPC} in this calculation assuming $N_R=0$, show a fall off at a low frequency simply due to an increment of deeply lying states. On the other hand, in the high-frequency region the spectrum agrees well with that for $N_D=0$. It was confirmed that this feature remained unchanged against temperature variation.

C. Comparison with experimental results

This section summarizes the quantitative interpretation of the MPC experiments performed on a-Si:H. A 6-μm-thick sample of intrinsic a-Si:H deposited on a glass substrate was used in the experiments. The contacts were coplanar Al electrodes evaporated on top of the film. The sample was homogeneously illuminated by 679-nm light from a diode laser. The light intensity was modulated sinusoidally at a frequency varying between $\omega/2\pi=10\,\mathrm{Hz}$ and 40 MHz. The MPC amplitude was detected by a standard lock-in amplifier for low frequencies (<100 kHz) or by an rf spectrum analyzer for high frequencies (>10 kHz). Further details of the experiments are given in our previous papers.[9,10] The present work extends the temperature range from 140 to 380 K. The drift-mobility data presented below were obtained in the linear response regime.

Figure 9 displays the measured MPC mobility against frequency at various temperatures. The kink expected from the

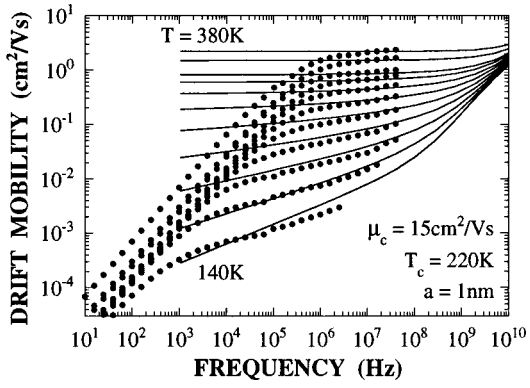

FIG. 9. Theoretical fits (lines) to the drift-mobility spectra obtained from MPC experiments for a-Si:H (dots). The eleven plots correspond to $T=140$, 160, 180, 200, 220, 240, 260, 280, 296, 340, and 380 K. The calculation assumes that $\mu_c=15\,\mathrm{cm}^2/\mathrm{V\,s}$, $T_c=220\,\mathrm{K}$, and $a=1\,\mathrm{nm}$.

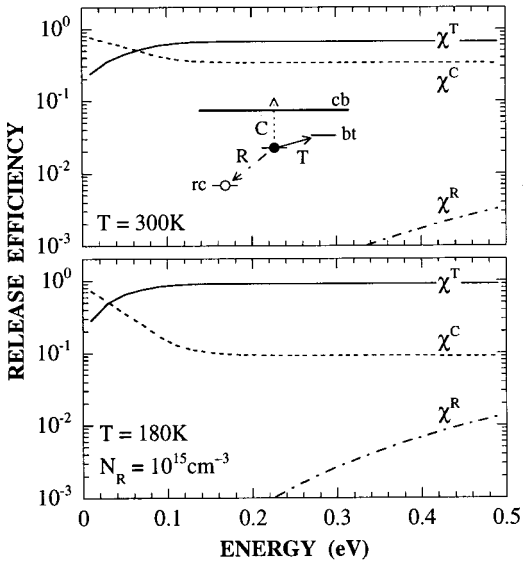

FIG. 10. Release efficiencies χ_i^C, χ_i^T, and χ_i^R as a function of energy. The calculation assumes that $N_R=10^{15}\,\mathrm{cm}^{-3}$. The upper and lower figures correspond to $T=300$ and 180 K, respectively. The relevant transitions are shown schematically in the inset.

numerical calculations is clearly identified in these spectra. In the experiments, we observed that the low-frequency fall-off is affected appreciably by varying the background illumination intensity, which presumably modifies the occupation of deep states, while the high-frequency part stays unchanged. The high-frequency MPC mobility is therefore justifiably interpreted as the drift mobility, which is independent of recombination as well as deep trapping. The experimental data in the high-frequency regime were first compared with the numerical results based on Eq. (27) with $N_R=N_D=0$. For $T\geqslant 160\,\mathrm{K}$, excellent agreement was obtained between theory and experiment, leading to the estimates that $\mu_c=15\,\mathrm{cm}^2/\mathrm{V\,s}$ and $T_c=220\,\mathrm{K}$. However, the drift mobility measured at the lowest temperature $T=140\,\mathrm{K}$ is several times larger than the theoretical prediction, which postulates that photocurrent is carried only by band electrons. This discrepancy leads us to consider the hopping transport of band-tail electrons. The theoretical analysis for hopping mobility is described in Appendix C. Numerical results involving the contribution from hopping mobility are in reasonable agreement with experiment, as shown by the solid lines in Fig. 9.

D. Steady state

Finally, we discuss the steady-state properties. Figure 10 shows the release efficiencies χ_i^C, χ_i^T and χ_i^R calculated as a function of energy for $N_R=10^{15}\,\mathrm{cm}^{-3}$. We learn from the figure that thermal emission into the conduction band gives a sizable contribution only in the close vicinity of the band edge. Apart from that, tunneling transitions into the band-tail states are the most probable release process, even for room temperature. The dominance of intra-band-tail transitions is more pronounced at lower temperatures. The efficiency of recombination transitions, which is nearly visible on the deep-energy side in this plot, increases with decreasing temperature. Recall that recombination transitions are almost temperature independent. In effect, the low-temperature behavior reflects the deactivation of the other two transition channels. The observation that $\chi_i^R\ll 1$ implies that the steady-state occupation function $\overline{f_i}$ does not much deviate from the Boltzmann form $f_i^{\mathrm{eq}}=\exp[-(\varepsilon_i-\varepsilon_{fn})/kT]$. This is confirmed in Fig. 11, where the occupancy ratios, $\overline{f_i}/f_i^{\mathrm{eq}}$ computed at $T=180\,\mathrm{K}$, are plotted for various densities of recombination centers. A significant deviation is observed only for $N_R=10^{17}\,\mathrm{cm}^{-3}$.

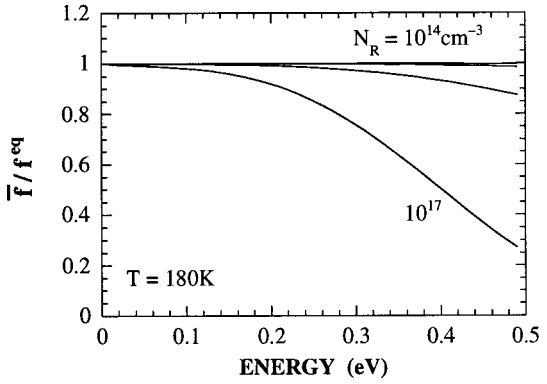

FIG. 11. Ratios of the steady-state occupancy $\overline{f_i}$ to the Boltzmann occupancy f_i^{eq} at $T=180\,\mathrm{K}$ for various values of N_R.

Figure 12 illustrates the recombination efficiencies η^C and η^T calculated as a function of temperature. It was confirmed that these numerical results were essentially unaffected by varying the density of recombination centers in the range $N_R\leqslant 10^{17}\,\mathrm{cm}^{-3}$. From this figure, one finds that the tunneling transitions contribute an increasing amount to the recombination process as temperature is reduced. An efficiency η^C lower than unity, as shown here, means that a substantial enhancement of recombination takes place, as described by the effective capture coefficient $C_{\mathrm{eff}}=C/\eta^C$, as well as by the relevant band electron lifetime $\overline{n}/\overline{G}=1/C_{\mathrm{eff}}N_R$. The theoretical results agree with a variety of experiments, such as photoluminescence,[12,13] photoinduced

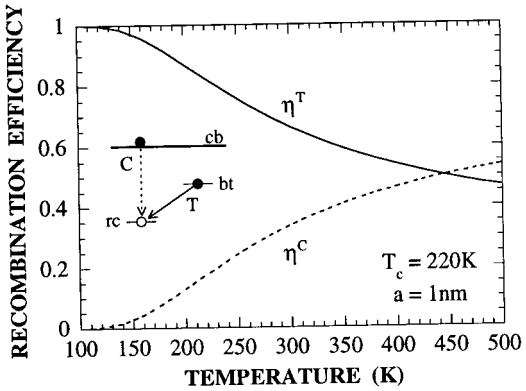

FIG. 12. Recombination efficiencies η^C and η^T calculated as a function of temperature for $N_R=10^{15}\,\mathrm{cm}^{-3}$. The relevant transitions are shown schematically in the inset.

absorption,[7] light-induced electron spin resonance,[19] and steady-state photoconductivity,[21] all of which show that recombination in *a*-Si:H is dominated by tunneling at low temperatures. Even for room temperature, the present calculations indicate that tunneling transitions account for about $\frac{2}{3}$ of the total recombination rate. This conclusion is supported by room-temperature observation of the spin-dependent photoconductivity, which can be explained when the majority of photocarriers undergo the tunneling recombination,[22] and throws doubt on the conventional interpretation, which assumes direct capture into recombination centers in such a high-temperature regime.

IV. SUMMARY

This paper presents a theoretical description of carrier thermalization and recombination, which, in a unified manner, takes into account tunneling interactions between localized states as well as thermal interactions between localized and extended states. Numerical results expressed in Fourier space are discussed intensively for the purpose of achieving a quantitative interpretation of the frequency dependent drift mobility measured for *a*-Si:H. The incorporation of tunneling transitions, with the accepted value for the localization radius, yields appreciable effects, namely, an accelerated thermalization of nonequilibrium electrons in the conduction band tail as well as a reduced magnitude of the drift mobility reflecting the energy distribution of these electrons. The theory, augmented by involving a low-temperature hopping transport, shows excellent agreement with experiments performed over a wide range of frequencies and temperatures. The other important role played by tunneling transitions is to provide additional recombination channels through localized states in parallel with direct capture of band electrons. The numerical calculations suggest that even for room temperature, the tunneling transitions accounts for about $\frac{2}{3}$ of the steady-state recombination rate. On the basis of these observations, this work argues against the conventional interpretation that assumes multiple trapping in the band tail and recombination by direct capture.

APPENDIX A: UPWARD AND DOWNWARD TRANSITIONS

In the continuum limit, the survival probability against tunneling transitions $S^T(\varepsilon,t)$ can be represented analytically as

$$S^T(\varepsilon,t)=\exp\{-\pi a^3 D(\varepsilon) kT_c[F_\downarrow(t)+F_\uparrow(\varepsilon,t)]\}, \tag{A1}$$

with the exponential density of states $D(\varepsilon)=D_c\exp[-(\varepsilon_c-\varepsilon)/kT_c]$. The time evolution is governed by the function $F_\downarrow(t)$, which involves only downward transitions and is energy independent, and the function $F_\uparrow(\varepsilon,t)$, which involves only upward transitions and is energy dependent. They are written as

$$F_\downarrow(t)=V_0(t)/\pi a^3, \tag{A2}$$

$$F_\uparrow(\varepsilon,t)=\frac{\gamma}{\gamma-1}\nu_0 t\times\begin{cases}\exp\left((\gamma-1)\dfrac{\varepsilon_c-\varepsilon}{kT}\right)-1, & \nu_0 t<1,\\ \exp\left((\gamma-1)\dfrac{\varepsilon_c-\varepsilon}{kT}\right)-\dfrac{A(t)}{\nu_0 t}, & \\ \qquad 1<\nu_0 t<\exp\left(\dfrac{\varepsilon_c-\varepsilon}{kT}\right)\end{cases} \tag{A3}$$

where $\gamma=T/T_c$ and the function $A(t)$ is expressed for $\gamma\neq 1$ as

$$A(t)=\sum_{k=0}^{4}\frac{[\ln(\nu_0 t)]^k}{k!}+\frac{1}{\gamma^4}\sum_{k=5}^{\infty}\frac{[\gamma\ln(\nu_0 t)]^k}{k!}.$$

It is easily found that $A(t)$ behaves as $\nu_0 t$ for $0\leqslant\ln(\nu_0 t)\ll 1$ and as $(\nu_0 t)^\gamma/\gamma^4$ for $\ln(\nu_0 t)\gg 1$. It is not important to consider the behavior at long times such that $\nu_0 t>\exp[(\varepsilon_c-\varepsilon)/kT]$, which is omitted from Eq. (A3), since the time range in which the tunneling transitions contribute significantly to the carrier release is limited, in competition with the thermal emission to extended states. A careful examination of Eqs. (A2) and (A3) shows that for $\gamma>\frac{1}{2}$ the upward transitions predominate, $F_\uparrow(\varepsilon,t)\gg F_\downarrow(t)$, for all times in the energy range below $\varepsilon_c-[kT/(\gamma-1)]\ln(2-1/\gamma)$.

APPENDIX B: MEAN-FIELD MODEL

A previous theory for carrier kinetics, called the mean-field model,[9] is based upon the use of the configurationally averaged tunneling transition rate $\Sigma_m\langle w_{nm}\rangle_m$, resulting in a formulation with linearly increasing tunneling volume $V_{ij}(t)=\pi a^3\nu_{ij}t$ for all times. It turns out that this overestimates tunneling interactions for long times, as compared with Eq. (13), which is derived from the more complete theoretical analysis.

It is informative to first examine analytical results for an exponential band tail. Within the framework of mean-field model, the functions $F_\downarrow(t)$ and $F_\uparrow(\varepsilon,t)$ involved in Eq. (A1) are simply expressed by

$$F_\downarrow(t)=\nu_0 t, \tag{B1}$$

$$F_\uparrow(\varepsilon,t)=\frac{\gamma}{\gamma-1}\nu_0 t\left[\exp\left((\gamma-1)\frac{\varepsilon_c-\varepsilon}{kT}\right)-1\right], \tag{B2}$$

for all times. In comparison with Eqs. (A2) and (A3), one easily finds that the mean-field approach becomes equivalent to the exact treatment when $\ln(\nu_0 t)\ll 1$. Even in the long-time region $1\ll\ln(\nu_0 t)\leqslant(\varepsilon_c-\varepsilon)/kT$, the same leading term is evaluated for $F_\uparrow(\varepsilon,t)$ from Eqs. (A3) and (B2) at high temperatures such that $\gamma>1$. Therefore, it can be said that the mean-field model forms a good approximation to the exact theory in the high-temperature regime insofar as the exponential density of states is concerned. However, it is evident that the similarity is no longer maintained at lower temperatures.

Figure 13 compares the survival probabilities $S_i(t)=S_i^C(t)S_i^T(t)$ calculated in accordance with the exact theoreti-

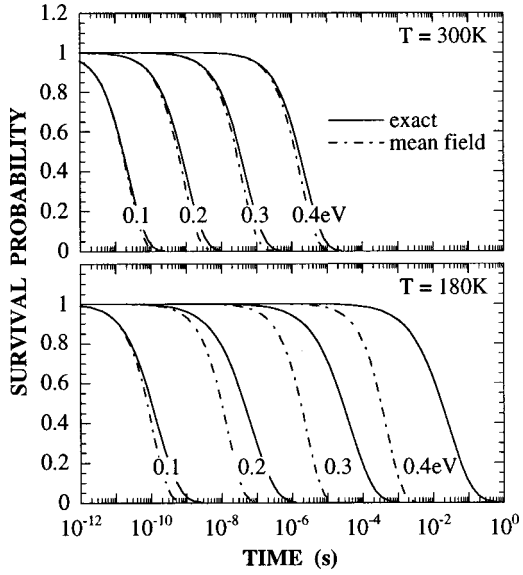

FIG. 13. Comparison between the survival probability for $a=1$ nm displayed in Fig. 1 (full lines) and that calculated in accordance with the mean-field model (chain-dotted lines).

cal analysis and the mean-field approximation. In the calculation, the density of states given by Eq. (36), with $T_c=220$ K, was assumed. As expected from analytical considerations, both results are nearly identical for $T>T_c$, while they show a significant deviation for $T<T_c$. Figure 14 illustrates the drift-mobility spectra computed for various temperatures and confirms the agreement in the high-temperature case $T>T_c$.

APPENDIX C: HOPPING TRANSPORT

Here, we consider low-temperature transport solely within the framework of the hopping model. The starting point of the theory is the rate equation[5,7]

$$\frac{d}{dt}f_n(t)=\sum_m f_m(t)w_{mn}-f_n(t)\sum_m w_{nm}, \tag{C1}$$

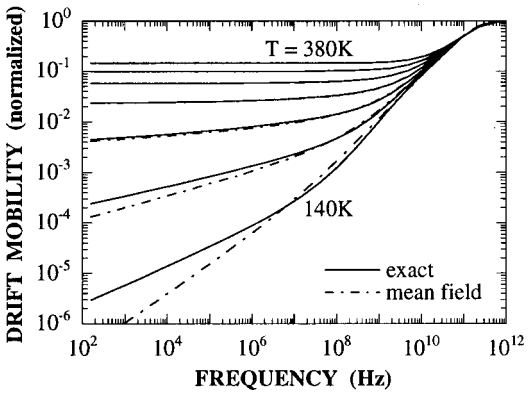

FIG. 14. Comparison between the drift mobility for $a=1$ nm displayed in Fig. 3 (full lines) and that calculated in accordance with the mean-field model (chain-dotted lines).

which neglects thermal interactions with extended states as well as recombination transitions. It is convenient for the analysis to express the solution formally as

$$f_n(t)=\sum_m f_m(0)g_{mn}(t), \tag{C2}$$

where the Green's function, $g_{mn}(t)$, corresponds to the probability of finding an electron at site n at time t given that it started from site m at $t=0$. The Green's function obeys the equation

$$g_{mn}(t)=\delta_{mn}s_n^T(t)+\sum_u \int_0^t dt' g_{mu}(t')w_{un}s_n^T(t-t'), \tag{C3}$$

where δ_{mn} is the Kronecker delta. Paralleling the statistical treatment applied in Sec. II, we arrive at the formulas for a discrete density of states given by

$$n_i(t)=N_i f_i(t)=\sum_j n_j(0)G_{ji}(t), \tag{C4}$$

$$G_{ji}(t)=\delta_{ji}S_i^T(t)+\sum_k \int_0^t dt' G_{jk}(t')C_{ki}(t-t')N_i S_i^T(t-t'). \tag{C5}$$

Here, $G_{ji}(t)$ is the sum of Green's functions configurationally averaged with level indexes j and i kept fixed, and symbolically expressed as

$$G_{ji}(t)=\sum_{n(i)} \langle g_{m(j)n(i)}(t)\rangle_{\{u\}},$$

where $n(i)$ denotes a site n that belongs to level i, and similarly $m(j)$ references level j. Isoenergetic terms such as $G_{ii}(t)$ and $C_{ii}(t)$ are included in Eqs. (C4) and (C5), which account for the transport path traversing states of the same energy. For consistency, the averaged survival probability against tunneling transitions $S_i^T(t)$ is now defined as exp $[-\Sigma_j N_j V_{ij}(t)]$, which involves the equal energy element $N_i V_{ii}(t)$ in the summation.

The hopping motion to be considered is isotropic for an ensemble of randomly positioned sites. Then, the square of site distance $\mathbf{r}_{mn}^2=(\mathbf{r}_n-\mathbf{r}_m)^2$ weighted by the transfer probability $g_{mn}(t)$ follows as

$$\mathbf{r}_{mn}^2 g_{mn}(t)=\sum_u \int_0^t dt'[\mathbf{r}_{mu}^2 g_{mu}(t')+g_{mu}(t')\mathbf{r}_{un}^2] \times w_{un}s_n^T(t-t'), \tag{C6}$$

where $\mathbf{r}_{mn}^2=(\mathbf{r}_{mu}+\mathbf{r}_{un})^2$. Performing the configurational average, we obtain

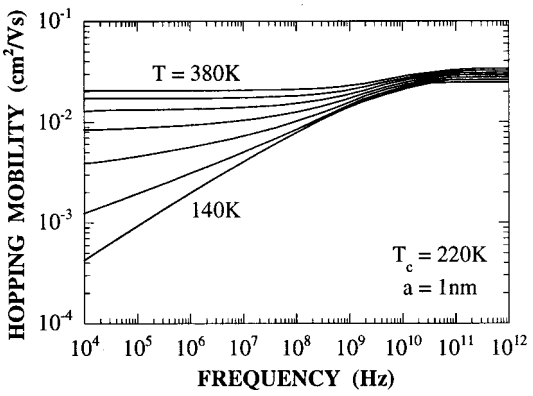

FIG. 15. Hopping mobility spectra calculated for various temperatures $T=140-380$ K.

$$R_{ji}^2(t)=\sum_{n(i)}\langle \mathbf{r}_{m(j)n(i)}^2 g_{m(j)n(i)}(t)\rangle_{\{u\}}$$
$$=\sum_k \int_0^t dt'[R_{jk}^2(t')C_{ki}(t-t')$$
$$+G_{jk}(t')B_{ki}(t-t')]N_i S_i^T(t-t'). \quad \text{(C7)}$$

The function $B_{ki}(t)$ is defined as

$$B_{ki}(t)=\exp\left(-\frac{\varepsilon_i-\varepsilon_k}{kT}\right)\frac{d}{dt}\int_0^\infty dr\,4\pi r^4\{1-\exp[-w_{ik}(r)t]\}, \quad \text{(C8)}$$

of which an approximate form is derived to be

$$B_{ki}(t)=3\pi a^5\exp\left(-\frac{\varepsilon_i-\varepsilon_k}{kT}\right)$$
$$\times\begin{cases}\nu_{ik}, & \nu_{ik}t<1,\\ \dfrac{1}{t}\displaystyle\sum_{p=0}^{4}\frac{[\ln(\nu_{ik}t)]^p}{p!}, & \nu_{ik}t>1\end{cases}$$

similar to the manner of evaluating the tunneling volume $V_{ij}(t)$. The mean-square displacement for all the traveling electrons is expressed in terms of $R_{ji}^2(t)$ as

$$R^2(t)=\frac{\sum_j n_j(0)\sum_i R_{ji}^2(t)}{\sum_j n_j(0)}. \quad \text{(C9)}$$

Its time derivative defines the diffusion coefficient,[5] and is related to the hopping mobility via the Einstein relation, $\mu_{\rm hop}(t)=(q/6kT)dR^2(t)/dt$.

The time-dependent hopping mobility $\mu_{\rm hop}(t)$ given above corresponds to the response function, which represents the transient decay of the system's conductivity following an impulse excitation at $t=0$, $\sigma_{\rm hop}(t)=qN(0)\mu_{\rm hop}(t)$. Therefore, it is interpreted as a time-domain drift mobility of an nonequilibrated ensemble of electrons with density $N(0)$. On the basis of population conservation, $N(t)=N(0)\theta(t)$, the time-domain drift mobility is converted into its frequency-domain counterpart by the relation,

$$\mu_{\rm hop}(\omega)=\frac{\mathcal{F}[\sigma_{\rm hop}(t)]}{\mathcal{F}[qN(t)]}=i\omega\mathcal{F}[\mu_{\rm hop}(t)]. \quad \text{(C10)}$$

The frequency-dependent hopping mobility $\mu_{\rm hop}(\omega)$ can be determined from solving Eqs. (C5) and (C7) in Fourier space. Inspecting Eq. (C9), we realize that the present theory is capable of calculating the hopping mobilities for various initial conditions, for example, a discrete excitation of certain levels as well as a uniform excitation over all the levels. An interband photogeneration, under which the initial occupation is established by capturing band electrons, favors the uniform excitation. In this case the occupation density $n_j(0)$ can be replaced with the level density N_j in Eq. (C9).

Figure 15 shows the hopping mobility spectra $|\mu_{\rm hop}(\omega)|$ calculated for various temperatures with the density of states given by Eq. (36). In comparison with Fig. 3 where the drift mobility $|\mu(\omega)|$ is computed on the basis of Eq. (27), we find that the hopping mobility exhibits a relatively weak thermal activation. It must be borne in mind that this is a pure hopping model derivation of $\mu_{\rm hop}(\omega)$. A direct comparison with $\mu(\omega)$ is not necessarily justified owing to this simplification but is thought to be reasonable when extended states are little populated with electrons and equivalently $|\mu(\omega)|/\mu_c\ll 1$. The drift mobility corrected with the hopping contribution $|\mu(\omega)+\mu_{\rm hop}(\omega)|$ is illustrated in Fig. 16. The band mobility $\mu_c=15\,\mathrm{cm^2/V\,s}$ was used in the calculation of $\mu(\omega)$. It is confirmed from the figure that the electron transport is well described by $\mu(\omega)$ over a wide temperature range, except for $T\leqslant 140$ K where hopping transport dominates.

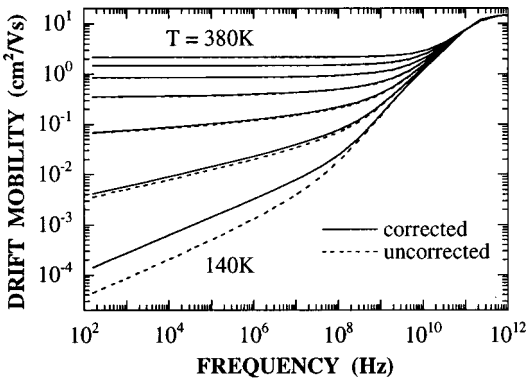

FIG. 16. Comparison between the drift mobility calculated for $\mu_c=15\,\mathrm{cm^2/V\,s}$ in accordance with Eq. (27) (dashed lines) and that corrected with hopping mobility shown in Fig. 15 (full lines).

[1] F. W. Schmidlin, Phys. Rev. B **16**, 2362 (1977).
[2] D. J. Dunstan, Philos. Mag. B **46**, 579 (1982).
[3] D. J. Dunstan, Philos. Mag. B **49**, 191 (1984).
[4] D. J. Dunstan, Philos. Mag. B **52**, 111 (1985).
[5] M. Grünewald, B. Movaghar, B. Pohlmann, and D. Würtz, Phys. Rev. B **32**, 8191 (1985).
[6] D. Monroe, Phys. Rev. Lett. **54**, 146 (1985).
[7] H. A. Stoddart, Z. Vardeny, and J. Tauc, Phys. Rev. B **38**, 1362 (1988).
[8] E. I. Levin, S. Marianer, and B. I. Shklovskii, Phys. Rev. B **45**, 5906 (1992).
[9] K. Hattori, M. Iida, T. Hirao, and H. Okamoto, J. Appl. Phys. **87**, 2901 (2000).
[10] K. Hattori, T. Hirao, M. Iida, and H. Okamoto, J. Non-Cryst. Solids **266–269**, 352 (2000).
[11] This relation is not justified in the degenerate case. However, it is unusual for *a*-Si:H because of relatively high density of localized states.
[12] R. A. Street, in *Semiconductors and Semimetals*, edited by J. I. Pankove (Academic, New York, 1984), Vol. 21B, pp. 197–244.
[13] D. J. Dunstan and F. Boulitrop, Phys. Rev. B **30**, 5945 (1984).
[14] The term ''monomolecular recombination'' represents recombination processes governed by population of a single type of carriers, which correspond to electrons in the context of the present discussion.
[15] R. A. Street, Philos. Mag. B **49**, L15 (1984).
[16] M. Abraham and V. Halpern, Philos. Mag. B **62**, 537 (1990).
[17] R. A. Street, J. Kakalios, and M. Hack, Phys. Rev. B **38**, 5603 (1988).
[18] C. E. Nebel, R. A. Street, N. M. Johnson, and J. Kocka, Phys. Rev. B **46**, 6789 (1992).
[19] K. Hattori, Y. Ota, K. Sato, and H. Okamoto, J. Appl. Phys. **84**, 4974 (1998).
[20] G. Schumm, W. B. Jackson, and R. A. Street, Phys. Rev. B **48**, 14 198 (1993).
[21] J.-H. Zhou and S. R. Elliott, Phys. Rev. B **48**, 1505 (1993).
[22] K. Lips, C. Lerner, and W. Fuhs, J. Non-Cryst. Solids **198–200**, 267 (1996).